NANO LETTERS

Letter

pubs.acs.org/NanoLett

Quantification of Deep Traps in Nanocrystal Solids, Their Electronic Properties, and Their Influence on Device Behavior

Deniz Bozyigit, Sebastian Volk, Olesya Yarema, and Vanessa Wood*

Department of Information Technology and Electrical Engineering, ETH Zurich, Gloriastr. 35, 8092 Zurich, Switzerland

Supporting Information

ABSTRACT: We implement three complementary techniques to quantify the number, energy, and electronic properties of trap states in nanocrystal (NC)-based devices. We demonstrate that, for a given technique, the ability to observe traps depends on the Fermi level position, highlighting the importance of a multitechnique approach that probes trap coupling to both the conduction and the valence bands. We then apply our protocol for characterizing traps to quantitatively explain the measured performances of PbS NC-based solar cells.

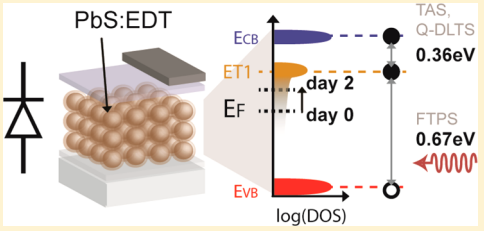

KEYWORDS: *Deep level transient spectroscopy (DLTS), thermal admittance spectroscopy (TAS), Fourier transform photocurrent spectroscopy (FTPS), quantum dots, PbS, photovoltaics*

Semiconductor (SC) materials derived from colloidally synthesized nanocrystals (NCs) are of high interest for applications in third-generation photovoltaics (PV), due to their promise of reduced production costs and potential for high power conversion efficiencies.[1−3] The current performance of NC solar cells still falls short of the requirement of 11−14% power conversion efficiency target needed to justify commercialization.[3] The low performance values for NC solar cells are often related to the presence of electronic trap states in the semiconducting NC solid, which act as recombination centers.[4−6] Chemical treatments aiming to passivate such trap states have improved solar cell performance and have led to the demonstration of 7.4% efficiency using PbS NCs.[6]

While most reports agree that trap states are present and limit performance, only recently has there been an effort to understand and quantify trap states experimentally[6−9] and theoretically.[6,10,11] In particular, the impact of trap states on basic electrical measurements such as current−voltage (IV) and capacitance−voltage (or admittance spectroscopy) remains poorly understood. Because such measurements are the most heavily employed for characterization of NC-based devices, understanding how trap states manifest themselves in these measurements would enable the systematic improvement of the NC materials and thin films to achieve high performance devices. Here, we demonstrate and validate a protocol for rapid characterization of trap states in NC solids that provides quantitative information about the number and energy of the trap states and relate our findings to key solar cell performance metrics such as open circuit voltage and short circuit current.

In our previous work, we applied current-based deep level transient spectroscopy (Q-DLTS) to a PbS NC solar cell (Figure 1a) and identified an abundant trap state manifold (T1) with an activation energy of E_{T1} = 0.40 eV.[9] In this work, we develop a consistent picture (Figure 1b) of the bulk traps in NC solids and their influence on the electronic behavior of a solar cell using Q-DLTS, thermal admittance spectroscopy (TAS), and Fourier transform photocurrent spectroscopy (FTPS) in conjunction with current voltage (IV) and photoluminescence (PL) measurements.

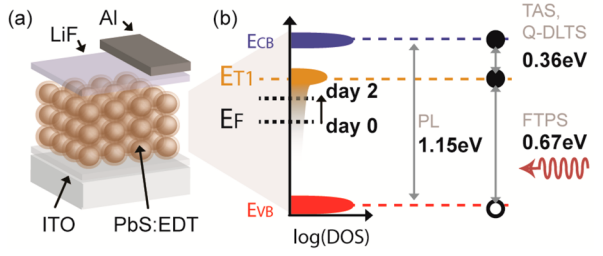

Figure 1. (a) Schematic of the Schottky junction solar cell. (b) Schematic of the density of states in the band gap of the PbS−EDT semiconductor, with the conduction band (blue), valence band (red), and the T1 trap manifold (dark orange). The experimental methods to determine energy offsets are indicated in gray. At day 0 the T1 traps are largely unoccupied, but a small change in the position of the Fermi level (E_F) over two days in air increases the occupation of the T1 traps.

For the experiments, we fabricate solar cells from PbS NCs in a diode structure with an ITO bottom anode and a LiF/Al/Ag top cathode (Figure 1a). The PbS NC thin film is deposited in air using a dipcoating procedure with an ethanedithiol (EDT) cross-linking step. The NCs used in this study show PL at 953 nm (1.30 eV) in solution (see Figure S1). Details of NC synthesis and the device fabrication procedure are given in ref 9. In the first step, we characterize the PV performance of our device by IV measurements under AM1.5G illumination. Our devices exhibit an open-circuit voltage of V_{oc} = 0.50 ± 0.06 V,

Received: July 27, 2013
Revised: October 18, 2013
Published: October 28, 2013

   dx.doi.org/10.1021/nl402803h | *Nano Lett.* 2013, 13, 5284−5288

short-circuit current of J_{sc} = 8.67 ± 0.67 mA/cm^2, fill factor of FF = 0.515 ± 0.006, and power conversion efficiency of η_{PCE} = 2.25 ± 0.18% with a fabrication yield of about 90%. The uncertainties are obtained from the measurement of seven equivalent devices (see Figure S2) and demonstrate that we are working with very reproducible devices—a prerequisite for the investigation of the device physics. To validate the quantitative agreement of the different trap characterization techniques, all data presented in this study is taken from one single device.

First, we determine the trap state density using Q-DLTS.[9] In such a measurement, the device is left at 0 V bias for 1 ms after which it is reverse-biased (−0.5 V) for 19 ms. The trapped charge is determined by integrating the current transient flowing out of the device. More details on the measurement technique are given in the Supporting Information and ref 9). Figure 2a shows the Q-DLTS spectra (ΔQ) for temperatures between 300 K (red) and 184 K (blue), exhibiting a peak charge of 7.4 nC/cm^2. We measure a PbS film thickness d = 70 nm by atomic force microscopy to relate this charge to a T1 trap density of 2.7 × 10^{16} cm^{-3}. This measurement, which we will refer to as the day 0 measurement, is performed under vacuum, following air exposure for 5 min, 1 h after evaporation of the top electrode. Repeating the same experiment two days later during which time the sample is stored in air (day 2 measurement), we find that the trapped charge increases 6-fold to 51 nC/cm^2 (Figure 2b). This corresponds to a T1 trap density of 1.8 × 10^{17} cm^{-3} and an activation energy of E_{T1} = 0.36 eV. The discrepancy to the previously reported[9] 0.40 eV results from an improved data analysis method, rather than a change in the measurement results. The improved method is discussed in the Supporting Information and is validated by the excellent agreement to the activation energy measured using TAS as presented below.

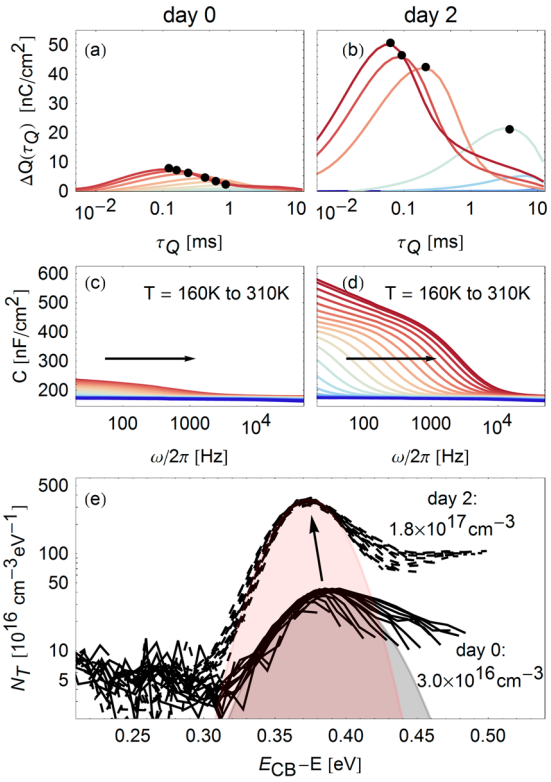

Figure 2. Q-DLTS spectrum for measurements on the device (a) immediately after fabrication and (b) after storage in air for two days. Spectra from 300 K (red) to 184 K (blue) are plotted. Black dots indicate the peak position that is used to determine the activation energy of the trap. (c, d) Thermal admittance spectroscopy (TAS) data for an applied bias voltage of 0 V. (e) Trap state density (N_T) determined by TAS. Fitting a Gaussian (shading) to the discrete trap state reveals a T1-trap state density of 3.0 × 10^{16} cm^{-3} at day 0 and 1.8 × 10^{17} cm^{-3} at day 2, centered at an energy of E_{T1} = 0.37 eV. This is in excellent agreement with the properties of the T1 manifold determined by Q-DLTS (2.7 × 10^{16} cm^{-3} at day 0 and 1.8 × 10^{17} cm^{-3} at day 2, with E_{T1} = 0.36 eV).

Next, we determine how the capacitance of the diode is influenced by the T1 trap. The capacitance is measured at 0 V bias with an impedance analyzer using a modulation amplitude of 10 mV (more details are given in the Supporting Information). We perform this measurement at temperatures between 160 K (blue) and 310 K (red). This is known as thermal admittance spectroscopy (TAS). The real part of the capacitance is plotted in Figure 2c. At high frequencies, we observe a capacitance of 175nF/cm^2. We relate this value to the geometric capacitance $C_{geo} = \epsilon_r\epsilon_0/d$, where ϵ_0 is the electric constant, because, for d = 70 nm, we obtain a relative dielectric constant of ϵ_r = 14, which is in good agreement with other reports.[12,13] On day 0, we observe a small increase in capacitance of up to 65 nF/cm^2 at frequencies below 1 kHz. Figure 2d shows the same measurement on day 2, where the additional low frequency capacitance is much larger and exceeds 300 nF/cm^2.

This capacitance increase at low frequencies is indicative of a deep trap state. A method developed by Walter et al.[14] allows the reconstruction of the density of trap states in the band gap (N_T) from TAS measurements (see Figure 2e). In Figure S3 we plot the derivative the TAS data to determine the reduced attempt-frequency of ν_{00} = 1.2 × 10^5 s^{-1}·K^{-2} (or an attempt-frequency of ν_0 = 1.07 × 10^{10} s^{-1} at 300 K). The attempt-frequency ν_0 represents how often a trapped carrier tries to escape to a conduction band state and is therefore an important metric for describing how a trap state interacts with the host semiconductor material. A previous attempt on TAS on PbS NC solids did not measure the attempt-frequency but estimated it to be on the order of 10^8 s^{-1}.[6] In other thin-film absorber materials, such as CIGS, attempt frequencies are often significantly larger (10^{11}−10^{12} s^{-1}).[14] This implies that the PbS NC thin-film has a lower density of conduction band states, that the traps interact more weakly with the conduction band, or a combination of both.

Using the TAS data and the attempt frequency, we plot in Figure 2e the trap density (N_T) versus energy depth from the conduction band, assuming a built-in voltage of 0.6 V. The data shows a discrete trap state, which we fit by a Gaussian distribution (shading in Figure 2e). From the fit we obtain a density of N_{T1} = 3.0 × 10^{16} cm^{-3} and E_{T1} = 0.39 eV on day 0 and N_{T1} = 1.8 × 10^{17} and E_{T1} = 0.37 eV on day 2, in excellent agreement with the Q-DLTS values. The width of the Gaussian distributions are on the order of the thermal energy (σ = 20−28 meV), so we conclude that thermal broadening is limiting the energy resolution of the measurement. We note that the systematic uncertainty on the energy scale is on the order of 25 meV due to the uncertainties in the measured sample temperature. In addition to the discrete T1-trap manifold, N_T features a plateau that extends further into the middle of the band gap (0.4−0.5 eV). These states also appear in the DLTS measurements as the broad shoulder at long time constants in high-temperature spectra (see Figure 2b). The fact that this

dx.doi.org/10.1021/nl402803h | Nano Lett. 2013, 13, 5284−5288

shoulder appears only at high temperatures at long time constants and is broad in shape is compatible with a distribution of midgap states. Scanning tunneling spectroscopy measurements on EDT-treated PbS NC-films have recently found a similar density of states.[15]

Further agreement between Q-DLTS and TAS is found in the value for the trap capture cross section (σ_{T1}). Like the attempt frequency, σ_{T1} quantifies the interaction of the trap states with mobile carriers. It can be determined for both TAS and Q-DLTS measurements as shown in the Supporting Information. The cross sections derived from TAS ($\sigma_{T1,TAS}$ = 3.7×10^{-16} cm^2) and from DLTS ($\sigma_{T1,DLTS}$ = 6.0×10^{-16} cm^2) correspond to a disc with a capture radius of 110−140 pm. We note that this value is in the range of the ionic radius of most metal ions (50−130 pm),[16] which suggests a possible origin for the observed traps. The fact that the extracted capture radius is physically reasonable justifies the use of the effective mass approximation in the Q-DLTS and TAS data analysis (see Supporting Information). Although this approximation was originally developed in the context of band transport semiconductors, our results show that it is applicable to NC solids to describe trap dynamics.

On first consideration, the strong quantitative agreement of Q-DLTS and TAS measurements may not be surprising as both techniques are based on charge measurements in the dark. In fact, in some cases, time-domain and frequency-domain measurements are equivalent and are trivially related by the Fourier transform.[17] However, for Q-DLTS and TAS, this is not the case. Q-DLTS is a large-signal technique where the total amount of trapped charge is directly measured (in units of cm^{-3}). In contrast, TAS is a small-signal technique and requires an analytical model of the band bending in the device to provide the spectral density of trapped charge (in units of cm^{-3}·eV^{-1}). Therefore, the agreement in the quantity and energy of traps found with Q-DLTS and TAS is significant. Q-DLTS validates the assumptions needed for TAS analysis, which is an important step toward a consistent model of charge transport in NC-based devices.

Traps are particularly detrimental to photovoltaic performance if they are coupled to both the valence band (VB) and the conduction band (CB) and therefore act as recombination centers. Q-DLTS and TAS measurements consistently show trap states with an activation energy of E_{T1} = 0.36 eV, which we interpret as the energy distance to the CB. Our measurements do not allow us to discriminate whether the T1 trap is close to the VB or the CB. We tend to think that it is close to the CB based on the measurements in ref 18. In contrast, ref 15 indicated that the dominant trap states are closer to the VB.

We test the coupling of this T1 trap manifold to the VB using the Fourier transform photocurrent spectroscopy (FTPS) technique (see Figure 3a).[19] In this technique, we measure the photocurrent spectrum by illuminating the device with infrared light from an FTIR spectrometer (more experimental details are given in the Supporting Information). The photocurrent plotted in Figure 3b shows a distinct peak at 0.67 eV. Given the band gap for this NC-solid of 1.0−1.2 eV determined by PL (Figure 3b red), 0.67 eV matches the expected energy for the T1−VB transition. We therefore conclude that the T1 traps couple efficiently to both the VB and the CB and can therefore act as recombination centers.

The peak in the subbandgap photocurrent that we measure with FTPS is on the order of 5.3pA on day 0 (solid black line in Figure 3b) and reduces by 16% on day 2 (dashed black line).

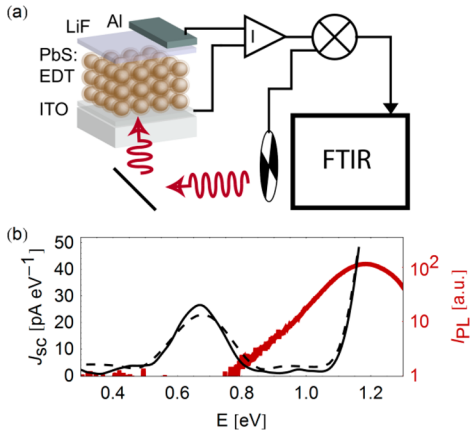

Figure 3. (a) Experimental setup for FTPS measurements. Under infrared illumination, the photocurrent is measured and recorded by a Fourier transform infrared spectrometer (FTIR). (b) Photoluminescence spectrum of the NC-solid (red, right axis) and photocurrent (left axis) for day 0 (solid black line) and day 2 (dashed black line). PL peak at 1.15 eV determines the effective band gap of the semiconductor. The photocurrent shows a transition at 0.67 eV, which is consistent with the energetic position of the T1 trap measured with Q-DLTS and TAS.

This reduction is accompanied by a shift to higher energies that is on the order of 10 meV (see Figure S4b). The decrease in photocurrent magnitude and the shift in energy is surprising and at first seems to contradict the apparent increase in traps under air exposure observed with Q-DLTS and TAS measurements. However, a consistent picture for device behavior can be developed that uses the concept of a partially filled trap band proposed in ref 18. As sketched in Figure 1b, if, at day 0, the Fermi level is lower in energy than the center of the T1 trap manifold, the T1 trap manifold will be largely unoccupied. Indeed, through electrical measurements (Q-DLTS, TAS), we observe a relatively small density of traps at the 0.36 eV transition to the CB. A shift in Fermi level such that a greater fraction of traps is occupied in thermal equilibrium on day 2 than on day 0 explains the larger Q-DLTS and TAS signals measured on day 2. Furthermore, because this shift in Fermi level would also mean that fewer trap states are available for absorption to take place, the shift is consistent with the decrease and shift to higher energy of the FTPS signal. From our measurements of the trap occupation on day 0 (N_{d0}) and day 2 (N_{d2}), we can estimate a 50 meV change in the Fermi level (ΔE_F) using Boltzmann statistics: N_{d2}/N_{d0} = 6.7 = $\exp(\Delta E_F/kT)$, where kT is the thermal energy.

This shift could arise from exposure to water or oxygen as the sample sits in air. We note that oxidation of the PbS would tend to lower the Fermi level instead of increase it.[20] This suggests either (1) that the trap state manifold is closer to the VB and that Q-DLTS and TAS probe the VB to trap transition while FTPS probes the trap state to CB transition such that our results should be explain by a decrease in the Fermi level, or (2) that the change in Fermi energy is not due to oxidation of PbS but results from a more complex process. It was indicated by the work of Tang et al. that the degradation under air exposure is related to the Al electrode.[21] Recently it has been shown that n-type PbS NC solids can be obtained by the contact with a reducing agent,[22] which makes it plausible, that Al, as a strong reducing agent, could have a similar effect and slightly increase the Fermi energy upon degradation of the electrode.

dx.doi.org/10.1021/nl402803h | Nano Lett. 2013, 13, 5284−5288

To understand how trap states influence the device performance, we perform current−voltage (IV) measurements. Figure 4a shows nearly identical IV characteristics on day 0 (solid) and day 2 (dashed). Under AM1.5G illumination (Figure 4b), we observe that the open-circuit voltage (V_{oc}) does not change within the observation time of two days and that the short-circuit current (J_{sc}) decreases by 23% from 9.3 mA/cm^2 to 7.2 mA/cm^2.

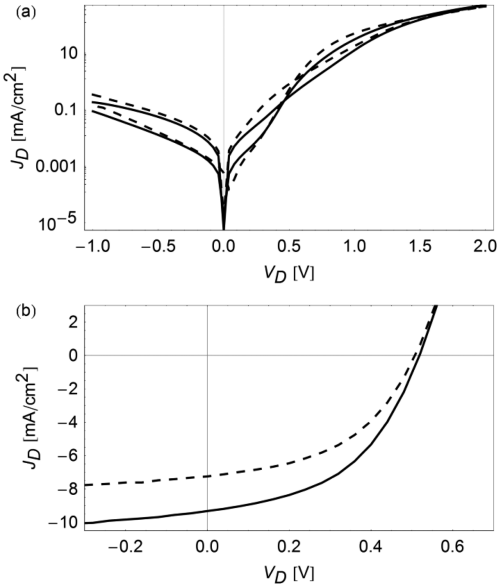

Figure 4. (a) Current−voltage characteristic in the dark at day 0 (solid) and at day 2 (dashed). (b) Current−voltage characteristic under AM1.5G illumination at day 0 (solid) and day 2 (dashed). We observe a slight reduction of the photocurrent at day 2, consistent with a change in the Fermi level in the semiconductor.

These observations are in line with the picture in which the occupation of the T1 trap manifold changes due to a shift in the Fermi level following exposure of the sample to air. First, the V_{oc} is limited by internal recombination and sensitive to the number of trap states.[3] We do not observe a change in V_{oc} from day 0 to day 2, which supports our conclusion that the total number of traps does not change significantly. Second, the reduction in J_{sc} indicates a reduced built-in field (F_{bi}). When the occupation of the trap states in the semiconductor changes, it is thermodynamically required to reduce the built-in field and thereby reduce J_{sc}. Assuming that $J_{sc} \propto F_{bi}$, we find that the observed reduction in J_{sc} by 23% would need a charge rearrangement of 24 nC/cm^2 (see Supporting Information). This is comparable to the change in trapped charge (43.6 nC/cm^2), which we observe in the Q-DLTS measurements. Thus, the change in our current−voltage characteristics is consistent with the internal rearrangement of charge that is observed through the three distinct measurements of the occupied trap states.

In summary, we have investigated trap states in PbS NC-based thin films and determined their influence on the electronic behavior of Schottky-type diodes. We implement three distinct measurements—Q-DLTS, TAS, and FTPS—and demonstrate that all agree quantitatively, showing a deep trap manifold (T1) with a density of $N_{T1} \geq 1.8 \times 10^{17}$ cm^{-3} and an activation energy to the CB of $E_{T1} - E_{CB} = 0.36$ eV. To our knowledge, the FTPS measurements are the first on NC solids and demonstrate that the traps interact efficiently with both the VB and the CB and can act as recombination centers in our solar cell. We leverage the change in measured trap densities in our device as a function of time to show that device aging in air results in a shift in the Fermi level and trap occupation rather than in the creation of additional traps. This new perspective on device degradation is consistent with the change in the IV characteristics of the diode. We also show that the T1 trap states are responsible for a large increase (up to 300 nF/cm^2) in the low frequency capacitance of the diode. This proves that the popular Mott−Schottky characterization technique is not in general applicable for NC solids.[12,13,23] Determination of the space charge region requires a more advanced technique, such as drive-level capacitance profiling (DLCP), that takes the low-frequency capacitance into account.[24]

Of the three measurement techniques we perform, TAS emerges as the most simple and robust technique to determine the density of states in the band gap of a solution processed NC solid. At the same time we find that trap states can be invisible to a TAS measurement depending on the occupation of the trap states due to the position of the Fermi level in the device. This can explain why earlier reports were not able to observe trap states using TAS.[6] Only in combination with a technique that probes the complementary transition—such as FTPS—can a definite account on the presence and quantity of trap states be given.

■ ASSOCIATED CONTENT

Ⓢ Supporting Information

Information on reproducibility of device fabrication, improved Q-DLTS data analysis, calculation of Q-DLTS and TAS parameters, additional information on FTPS measurements, and estimation of field reduction by trapped charges. This material is available free of charge via the Internet at http://pubs.acs.org.

■ AUTHOR INFORMATION

Corresponding Author

*E-mail: vwood@ethz.ch, phone: +41-44-632 66 54.

Author Contributions

D.B. fabricated devices and performed all measurements. S.V. built the FTPS measurement setup. O.Y. synthesized the materials. D.B. and V.W. envisioned the experiments. The manuscript was written through contributions of all authors.

Notes

The authors declare no competing financial interest.

■ ACKNOWLEDGMENTS

This research was supported by the Swiss National Science Foundation through grant 200021_135432 and the National Centre of Competence in Research Quantum Science and Technology.

■ ABBREVIATIONS

Q-DLTS, charge DLTS; TAS, thermal admittance spectroscopy; IV, current−voltage characteristics; FTPS, Fourier transform photocurrent spectroscopy; PL, photoluminescence; NC, nanocrystal; PV, photovoltaic; SC, semiconductor; EDT, ethanedithiol; ITO, indium−tin−oxide; VB, valence band; CB, conduction band; CIGS, copper indium gallium sulfide; DLCP, drive-level capacitance profiling

REFERENCES

(1) Sargent, E. H. *Adv. Mater.* **2008**, *20*, 3958−3964.
(2) Talapin, D. V.; Lee, J.-S.; Kovalenko, M. V.; Shevchenko, E. V *Chem. Rev.* **2010**, *110*, 389−458.
(3) Lunt, R. R.; Osedach, T. P.; Brown, P. R.; Rowehl, J. A.; Bulović, V. *Adv. Mater.* **2011**, *23*, 5712−27.
(4) Kramer, I. J.; Sargent, E. H. *ACS Nano* **2011**, *5*, 8506−14.
(5) Szendrei, K.; Speirs, M.; Gomulya, W.; Jarzab, D.; Manca, M.; Mikhnenko, O. V.; Yarema, M.; Kooi, B. J.; Heiss, W.; Loi, M. A. *Adv. Funct. Mater.* **2012**, *22*, 1598−1605.
(6) Ip, A. H.; Thon, S. M.; Hoogland, S.; Voznyy, O.; Zhitomirsky, D.; Debnath, R.; Levina, L.; Rollny, L. R.; Carey, G. H.; Fischer, A.; Kemp, K. W.; Kramer, I. J.; Ning, Z.; Labelle, A. J.; Chou, K. W.; Amassian, A.; Sargent, E. H. *Nat. Nanotechnol* **2012**, *7*, 577−82.
(7) Konstantatos, G.; Sargent, E. H. *Appl. Phys. Lett.* **2007**, *91*, 173505.
(8) Erslev, P. T.; Chen, H.-Y.; Gao, J.; Beard, M. C.; Frank, A. J.; van de Lagemaat, J.; Johnson, J. C.; Luther, J. M. *Phys. Rev. B* **2012**, *86*, 155313.
(9) Bozyigit, D.; Jakob, M.; Yarema, O.; Wood, V. *ACS Appl. Mater. Interfaces* **2013**, *5*, 2915−9.
(10) Voznyy, O.; Thon, S. M.; Ip, A. H.; Sargent, E. H. *J. Phys. Chem. Lett.* **2013**, 987−992.
(11) Kim, D. D.-H.; Lee, J.-H.; Grossman, J. C. *Phys. Rev. Lett.* **2013**, *110*, 196802.
(12) Luther, J. M.; Law, M.; Beard, M. C.; Song, Q.; Reese, M. O.; Ellingson, R. J.; Nozik, A. J. *Nano Lett.* **2008**, *8*, 3488−92.
(13) Clifford, J. P.; Johnston, K. W.; Levina, L.; Sargent, E. H. *Appl. Phys. Lett.* **2007**, *91*, 253117.
(14) Walter, T.; Herberholz, R.; Muller, C.; Schock, H. W. *J. Appl. Phys.* **1996**, *80*, 4411.
(15) Diaconescu, B.; Padilha, L. A.; Nagpal, P.; Swartzentruber, B. S.; Klimov, V. I. *Phys. Rev. Lett.* **2013**, *110*, 127406.
(16) Shannon, R. D. *Acta Crystallogr., Sect. A* **1976**, *32*, 751−767.
(17) Barnes, P. R. F.; Miettunen, K.; Li, X.; Anderson, A. Y.; Bessho, T.; Gratzel, M.; O'Regan, B. C. *Adv. Mater.* **2013**, *25*, 1881−1922.
(18) Nagpal, P.; Klimov, V. I. *Nat. Commun.* **2011**, *2*, 486.
(19) Vanecek, M.; Poruba, A. *Appl. Phys. Lett.* **2002**, *80*, 719.
(20) Zarghami, M. H.; Liu, Y.; Gibbs, M.; Gebremichael, E.; Webster, C.; Law, M. *ACS Nano* **2010**, *4*, 2475−85.
(21) Tang, J.; Wang, X.; Brzozowski, L.; Barkhouse, D. A. R.; Debnath, R.; Levina, L.; Sargent, E. H. *Adv. Mater.* **2010**, *22*, 1398−402.
(22) Koh, W.; Koposov, A. Y.; Stewart, J. T.; Pal, B. N.; Robel, I.; Pietryga, J. M.; Klimov, V. I. *Sci. Rep.* **2013**, *3*, 2004.
(23) Brown, P. R.; Lunt, R. R.; Zhao, N.; Osedach, T. P.; Wanger, D. D.; Chang, L.-Y.; Bawendi, M. G.; Bulović, V. *Nano Lett.* **2011**, *11*, 2955−61.
(24) Michelson, C. E.; Gelatos, A. V.; Cohen, J. D. *Appl. Phys. Lett.* **1985**, *47*, 412.

Supporting Information:

Quantification of Deep Traps in Nanocrystal Solids, their Electronic Properties, and their Influence on Device Behavior

Deniz Bozyigit[†], *Sebastian Volk*[†], *Olesya Yarema*[†], *Vanessa Wood*[†] *(*)*

†Department of Information Technology and Electrical Engineering, ETH Zurich, Gloriastr. 35, 8092 Zurich, Switzerland

PbS Nanocrystals

The PbS NCs used in this work were described previously in Ref. (1). For the convenience of the reader, in Figure S1 we provide a reproduction of a transmission electron microscopy (TEM) image and the absorption and photoluminescence (PL) spectra of NCs in solution. The exciton peak in the absorption spectrum is found at 820 nm (1.51 eV), while the PL peak is found at 953 nm (1.30 eV).

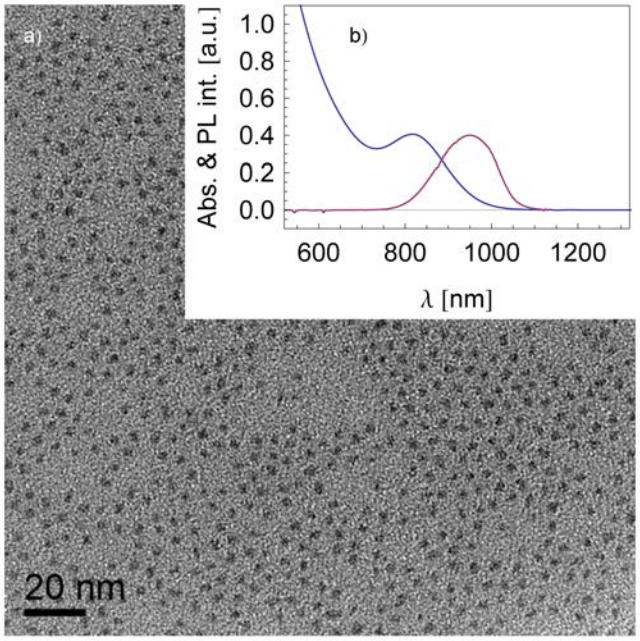

Figure S1: (a) TEM image of NCs (b) absorption spectrum (blue) and photoluminescence spectrum in solution (red). Reproduced from Ref. (1).

Device Reproducibility

In Figure S2, we show the current-voltage (IV) characteristics of 7 typical devices. In this fabrication run, a total of 8 devices were made. The 8th device showed poor IV characteristics, indicating a yield of close to 90%.

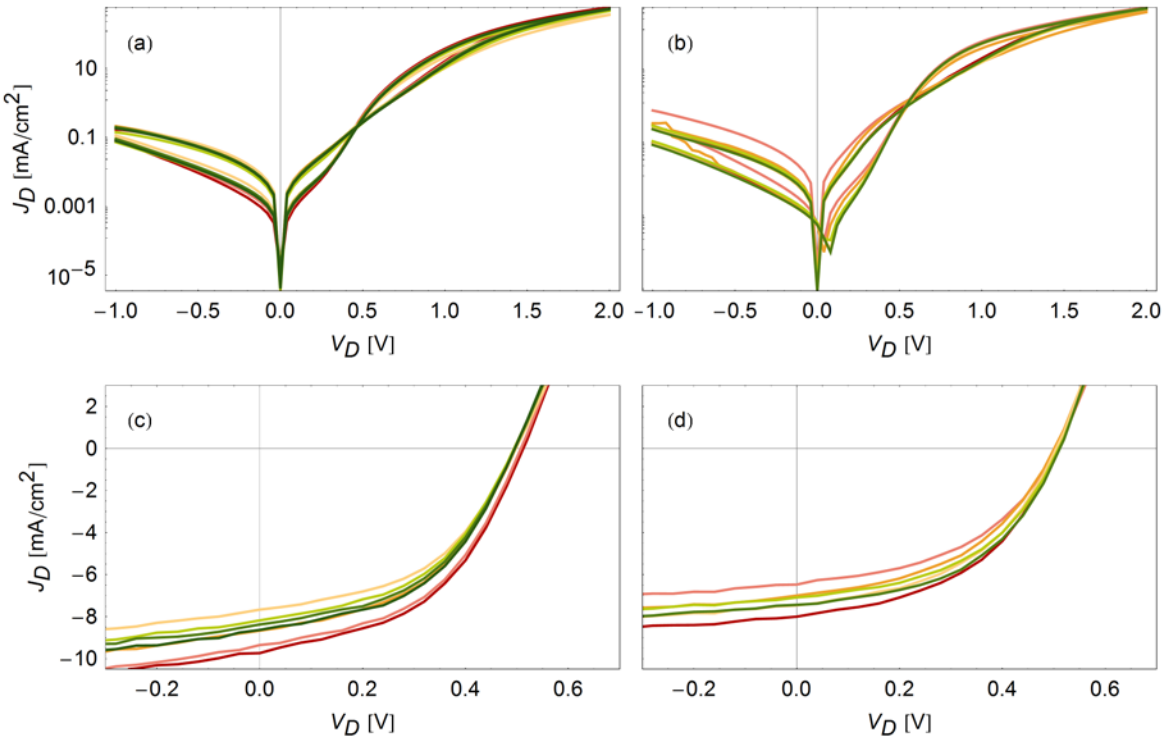

Figure S2: Current-voltage characteristics for 7 devices in the dark after fabrication (a) on day 0 and (b) on day 2, and under AM1.5G illumination (c) on day 0 and (d) on day 2.

Details on Device Fabrication and Handling

All measurements were performed on devices fabricated as described in Ref. (1), with an active area of $2.0\,\mathrm{mm}^2$. The PbS:EDT layer is deposited by dipcoating in air (30 layers). On top we evaporate a LiF/Al/Ag electrode in high vacuum, starting at a base pressure of $3\times10^{-7}\,\mathrm{mbar}$, and a maximum pressure during evaporation of $7\times10^{-7}\,\mathrm{mbar}$. Finally the samples are stored in a N_2 atmosphere. After short air exposure of 5 min, the sample is mounted into a cryostat (Janis ST-500), where it remains in vacuum for the following measurements: Q-DLTS, TAS, and IV. FTPS measurements are performed immediately afterwards in air. The sample is then left in air for two days.

Details Q-DLTS Measurements

The Q-DLTS measurements are performed according to the protocol described in detail in Ref. (1). The trap charging pulse used here has a voltage of $0\,\mathrm{V}$ and a length of $1\mathrm{ms}$, while the discharging takes place at a reverse bias of $-0.5\,\mathrm{V}$ for $19\,\mathrm{ms}$.

Improved Q-DLTS Data Analysis

The original proposal for DLTS by Lang is based on the concept of the rate window[2] and we used this approach in Ref. (1). Although the original method is based on the measurement of capacitance transients, we discuss current transients here. This is referred to as Q-DLTS and follows essentially the same mathematics.

The rate window is defined by a *detector time constant* τ_Q. The detector in DLTS is a system that outputs the correlation of the incoming transient to some internal test function – e.g. a

boxcar filter - that defines τ_Q. The output of the detector is the DLTS signal (ΔQ), which is sensitive to a particular decay rate τ_Q^{-1}. Faster and slower transients do not influence ΔQ.

In the original method, the detector was implemented in hardware and so ΔQ was calculated at the time of measurement (e.g. by a lock-in amplifier). Therefore there was only one fixed detector time constant τ_Q, and ΔQ was recorded as a function of the temperature T. The emission time constant of the trap τ_e changes with temperature, and, when $\tau_e = \tau_Q$, a peak is observed in $\Delta Q(T)$ at some temperature T_{peak}. To extract the activation energy of the trap state, an Arrhenius plot is constructed from data points of $\log(\tau_Q T_{peak}), 1/T_{peak}$.

Another approach, used in this work, was enabled by computer-based DLTS and is described in great detail in Ref. (3). At each temperature (*T)* the full transient is recorded and ΔQ is calculated after the measurement finishes. In this way a large number of points of $\Delta Q(\tau_Q)$ for any τ_Q can be obtained from each transient (See Figure 2a,b). In this plot of $\Delta Q(\tau_Q)$, the peak at position τ_{max} indicates the emission time and allows construction of an Arrhenius plot from the data points $\log(\tau_{max} T), 1/T$.

The activation energy extracted from both methods is equal in the case of ideal emission from a single discrete trap state. However, if processes other than carrier emission from traps are dependent on temperature, the two analysis methods are no longer equivalent. For example, if conduction in the material is temperature dependent, one might encounter a situation where at lower temperatures the peak in $\Delta Q(\tau_Q)$ changes in time and in height. In such a situation, it is possible that no peak would be visible in $\Delta Q(T)$.

We consider the peak in $\Delta Q(\tau_{\mathrm{Q}})$ of higher physical relevance, as it is obtained at a fixed temperature. Therefore we use the more recent analysis method in this paper. The extracted activation energy of 0.36 eV matches well with the results from thermal admittance spectroscopy (TAS) and deviates by $40\mathrm{meV}$ from the original analysis method reported in Ref. (1).

To determine the trap density, we previously integrated the complete current transient to determine the total number of emitted charges[1]. In this work, we use the method described in Ref. (3), where the trap density for a given trap type is determined by the peak in $\Delta Q(\tau_{\mathrm{Q}}) = \Delta Q_{\max}$:

$$N_{\mathrm{T}} = \frac{C_0 \Delta Q_{\max}}{eAd},$$

where *e* is the electron charge, *A* the device area, and *d* the film thickness. The factor C_0 results from the correlation technique using a boxcar-filter from time t_1 to time t_2 and is given by

$$C_0 = [\alpha^{1/(1-\alpha)} - \alpha^{\alpha/(1-\alpha)}]^{-1},$$

where $\alpha = t_2/t_1$. As we use $\alpha = 2$, in a typical experiment, this reduces to $C_0 = 4$.

Details on TAS Measurements

TAS measurements were performed directly after the DLTS measurements in identical conditions. For the TAS measurements, we measure the real and imaginary part of the capacitance for frequencies of $10\,\mathrm{Hz}$-$1\mathrm{MHz}$, at $0\,\mathrm{V}$ bias using a modulation amplitude of $10\mathrm{mV}$ with an impedance analyzer (Solartron MODULAB MTS). This measurement is performed continuously while we ramp down the temperature from $310\,\mathrm{K}$ to $160\,\mathrm{K}$ with a rate of $5\,\mathrm{K/min}$. The temperature is recorded at the sample for each capacitance value.

To reconstruct the trap density from the TAS data we employ the method developed by Walter *et al.*[4] In this method we use the real part (C_1) of the complex capacitance

$$C(\omega) = C_1(\omega) + iC_2(\omega),$$

where i is the imaginary number and ω is the angular frequency in s^{-1}. In the first step we calculate the following numerical derivative from the data

$$\frac{dC_1(\omega)}{d(\log\omega)} = \frac{\omega\, dC_1(\omega)}{d\omega},$$

which is plotted in Figure S3a for the day 2 measurement. A resonance peak of the T1-trap manifold can be observed in this data. The position of this peak is the *angular resonance frequency* , given by

$$\omega_0 = 2\nu_0 \exp\left(-\frac{\Delta E_T}{kT}\right),$$

where ν_0 is the angular *attempt-frequency* in units of s^{-1}, ΔE_T the trap activation energy, T is the temperature, k the Boltzmann constant. Although Walter neglects the temperature dependence of the attempt-frequency, we do include the temperature dependence according to the effective mass approximation and define the attempt frequency as $\nu_0 = \nu_{00}T^2$, where ν_{00} is the angular *reduced attempt-frequency* in units of $s^{-1}K^{-2}$. We plot the data in an Arrhenius-type plot (Figure S3b) to extract the reduced attempt-frequency by fitting the equation for the resonance frequency to the resonance peak ($y = 4.22x - 11.9$), which yields $\nu_{00} = 1.2\times10^5 s^{-1}K^{-2}$. To compare this number to other attempt-frequencies reported for other materials, we calculate the attempt-frequency at 300K to be $\nu_0 = 1.07\times10^{10} s^{-1}$.

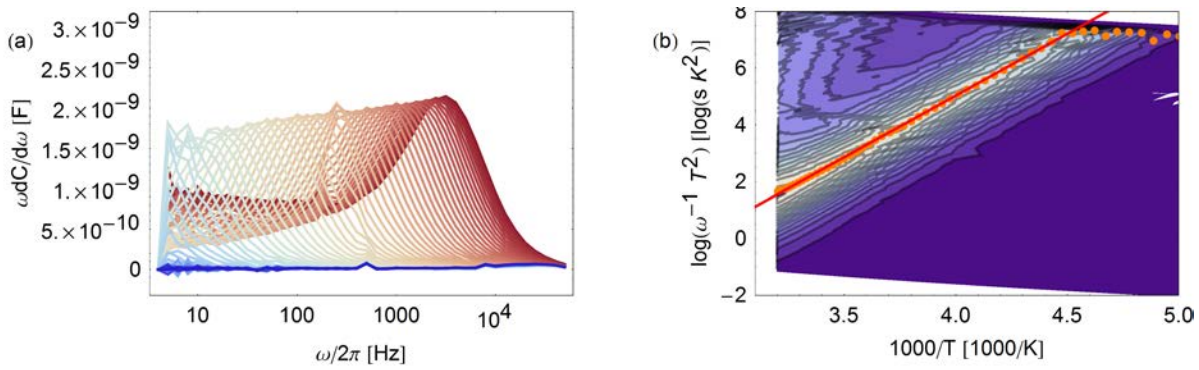

Figure S3: (a) Derivative of the real part of the capacitance, for temperatures between 160 K (blue) and 310 K (red). (b) Same data as in (a) shown in an Arrhenius-plot with extracted peak positions (orange dots) and fit of the resonance frequency (red line).

In the last step we perform a coordinate transformation on the data as proposed by Walter to obtain the spectral trap state density (N_T in $\mathrm{cm^{-3}eV^{-1}}$):

$$\left(\omega, \frac{\omega\, dC_1(\omega)}{d\omega}\right) \rightarrow \left(E, N_T\right), \text{ with}$$

$$E = kT \log \frac{2\nu_{00} T^2}{\omega} \quad \text{and} \quad N_T = \frac{{V_{\mathrm{bi}}}^2}{A \cdot W\left(eV_{\mathrm{bi}} - (E_{fn\infty} - E)\right)} \frac{1}{kT} \frac{\omega\, dC_1(\omega)}{d\omega},$$

where W is the depletion width, V_{bi} the built-in voltage, and $E_{fn\infty}$ the Fermi-energy position with respect to the conduction band. In our calculation, we assume a fully depleted film ($W = d = 70\mathrm{nm}$). Further, we assume $V_{\mathrm{bi}} = 0.6\mathrm{V}$ and $E_{fn\infty} = 0.6\mathrm{eV}$. The final result is plotted in Figure 2e in the main text.

Relating TAS and Q-DLTS (and calculation of cross sections)

Both theories for Q-DLTS and TAS measurements derive the dynamics of capture and emission processes of traps from the Shockley-Read-Hall (SRH) model. It is therefore possible to relate the parameters of the capture cross section (σ_{T}) in Q-DLTS and the attempt-frequency (ν_0) from TAS measurements. The emission time constant (τ_{e}) in the Q-DLTS method is given by

$$\tau_{\mathrm{e}} = \frac{1}{\sigma_{\mathrm{T}}\Gamma_{\mathrm{n}}T^2}\exp\left(\frac{\Delta E_{\mathrm{T}}}{kT}\right),$$

where T is the temperature, k the Boltzmann constant, ΔE_{T} the trap activation energy. Γ_{n} is a material and carrier dependent parameter given by $\Gamma_{\mathrm{n}} = \nu_{\mathrm{th}} N_{\mathrm{CB}} T^{-2}$. Here, ν_{th} is the thermal velocity of electrons and N_{CB} is the effective number of conduction band states according to equations in Ref. (3,5). For PbS NC-solids we have previously[1] estimated that $\Gamma_{\mathrm{n}} = 3.256\times10^{20}\,\mathrm{K^{-2}cm^{-2}s^{-1}}$.

To analyze TAS measurements, *Walter et. al.* use a linear differential equation to describe the evolution of the number of occupied traps. The part of this equation that describes carrier emission has the following form:

$$\frac{dn_t}{dt} = [\ldots] - \nu_0\, \mathrm{e}^{-\Delta E_t/kT}\, n_t\,,$$

where ν_0 is the angular *attempt-frequency* in units of $\mathrm{s^{-1}}$. The solution to this equation is an exponential decay, with a time constant of $\nu_0^{-1}\,\mathrm{e}^{\Delta E_t/kT}$. Identifying this time constant with the emission time constant of the Q-DLTS method, allows us to find the following relation:

$$\sigma_{\mathrm{T}}\Gamma_{\mathrm{n}}T^2 = \nu_0 = \nu_{00}T^2 = \sigma_{\mathrm{T}}\nu_{\mathrm{th}}N_{\mathrm{CB}}\,,$$

We can use this last equation to calculate an effective cross-section for the TAS measurements and find good agreement to the value obtained by DLTS.

Details on FTPS Measurements

The FTPS measurements were performed in air using a Bruker Virtex 80 FTIR spectrometer. For the sample illumination we use the built-in MIR lamp with the KBr beamsplitter and an additional filter (Si wafer, 500um, double sided polished). The sample holder is placed in the sample compartment of the spectrometer such that the infrared lightbeam (chopped at 278 Hz) is focused on the device. The photocurrent through the device is preamplified at 10^8 V/A using a FEMTO DLPCA-200 low current amplifier, which also provides a voltage bias to the sample. The preamplified signal is demodulated using the chopping frequency by a FEMTO LIA-MV-200 lock-in amplifier. The demodulated signal is fed to the FTIR spectrometer and recorded using the step-scan option of the device. A typical FTPS measurement consists of 226 interferometer steps, leading to a total measurement time of approximately 5 min.

Details on the Analysis of FTPS Measurements

We perform FTPS measurements on day 0 and day 2 and extract the total area under the photocurrent peak at 0.67eV. The peak is normalized to the band edge photocurrent to account for variations in illumination conditions between day 0 and day 2. We find that the photocurrent is reduced between 16% (at 0V bias) and 25% (at -1V bias) (See Figure S4a). Besides the reduction in photocurrent, we also observe that the peak energy, extracted from a Gaussian fit of the peak in the photocurrent spectrum, shifts to higher energies on the order of $10-20$meV (See Figure S4b). This is consistent with a shift in the Fermi level on the order of 40meV .

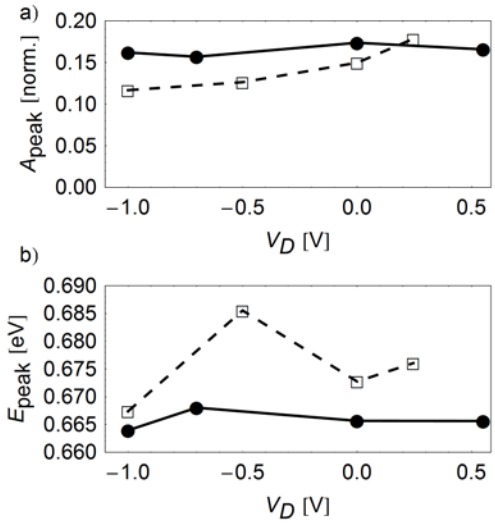

Figure S4: (a) Total photocurrent of the peak at 0.67V at day 0 (solid) and day 2 (dashed) for different bias voltages. (b) The energy of the photocurrent peak at day 0 (solid) and day 2 (dashed).

Estimation of Built-in Field Reduction

In this section, we show (1) how a reduction in short-circuit (J_{sc}) current can be explained by a reduced built-in field (F_{bi}) and (2) how much charge must be rearranged to obtain such a reduction in field.

First, we assume that the short-circuit current is a drift current, $J_{sc} = en\mu F_{bi}$ where e is the electron charge, n the charge carrier density, and μ the mobility. We take e, n, and μ to be constant. Second, we assume that the built-in voltage is essentially given by the work function difference between ITO (-4.8eV) and Al (-4.2eV) and therefore approximately $V_{bi} = 0.6\text{V}$.

For a semiconductor film of $70\,\text{nm}$, a change in J_{sc} of 23% thus relates to a change in field of $0.23 \cdot 0.6\,\text{V}/70\,\text{nm} = 19.7\,\text{kV/cm}$. To achieve this change in field in a material with a dielectric constant of 14, a charge of $14 \cdot \varepsilon_0 \cdot 19.7\,\text{kV/cm} = 24.4\text{nC/cm}^2$ needs to be displaced. This is indeed the approximate magnitude of the observed change in trap occupation of $43.6\,\text{nC/cm}^2$.

References:

(1) Bozyigit, D.; Jakob, M.; Yarema, O.; Wood, V. *ACS applied materials & interfaces* **2013**, *5*, 2915–9.

(2) Lang, D. V. *J. Appl. Phys.* **1974**, *45*, 3023.

(3) Gaudin, O.; Jackman, R. B.; Nguyen, T.-P.; Le Rendu, P. *J. Appl. Phys.* **2001**, *90*, 4196.

(4) Walter, T.; Herberholz, R.; Müller, C.; Schock, H. W. *J. Appl. Phys.* **1996**, *80*, 4411.

(5) Sze, S.; Ng, K. *Physics of semiconductor devices*; 2006.